



Thermodynamic properties of Ca–Pb electrodes determined by electromotive force measurements

Nathan D. Smith¹, Nicole E. Orabona¹, Jorge Paz Soldan Palma, Yuran Kong, Cameron Blanchard, Hojong Kim^{*}

Materials Science and Engineering, The Pennsylvania State University, 406 Steidle Building, University Park, PA, 16802, USA

HIGHLIGHTS

- Determined equilibrium cell potentials for a Ca–Pb electrodes.
- Established fundamental data for development of liquid Ca–Pb electrode.
- Resolved conflict in literature values for thermodynamic properties of Ca–Pb alloys.
- Provided comprehensive phase transition behavior for the Ca–Pb system.

ARTICLE INFO

Keywords:

Liquid metal batteries
Liquid metal electrodes
Calcium-lead alloys
Emf method
Ca–Pb phase diagram
Thermodynamic properties

ABSTRACT

Thermodynamic properties of Ca–Pb alloys are investigated by electromotive force (emf) measurements to determine equilibrium cell potentials and phase properties for their application in energy storage systems such as liquid metal batteries. Using the electrochemical cell $\text{Ca(s)} \mid \text{CaF}_2\text{(s)} \mid \text{Ca(in Pb)}$ at 700–1060 K, cell emf is measured for thirteen Ca–Pb alloys at mole fractions, $x_{\text{Ca}} = 0.06\text{--}0.80$. At 873 K, the equilibrium potentials of liquid Ca–Pb alloys are 0.57–0.62 V versus Ca and the activity values are as low as $a_{\text{Ca}} = 6.2 \times 10^{-8}$ at $x_{\text{Ca}} = 0.06$. In addition, the emf values as a function of temperature provide partial molar quantities (entropy and enthalpy) as well as phase transitions which are corroborated by determining transition temperatures and phase constituents using differential scanning calorimetry (DSC) and powder X-ray diffraction (XRD). This work establishes the fundamental data necessary for the design of Pb-containing liquid metal electrodes through the integration of electrochemical, thermal, and structural properties of Ca–Pb electrodes.

1. Introduction

As demand for grid-scale energy storage increases, low-cost earth-abundant electrode materials such as calcium become increasingly attractive. Despite the focus on lithium-based battery systems, thermodynamic analyses of liquid metal battery electrode couples indicate that calcium-based systems have higher equilibrium voltages than comparable Li-based systems [1,2]. The Ca–Pb electrode couple was suggested to be one of the more cost-efficient electrode material options (~ 36 \$ kWh^{−1}) for liquid metal batteries [2,3] based on the low costs of Ca (0.14 \$ mol^{−1}) and Pb (0.52 \$ mol^{−1}) and the cell voltage of Ca–Pb alloys from the measured thermodynamic properties at 1073 K by Delcet et al. [4]. Considering the practical operating temperature of liquid

metal batteries (<873 K) for energy storage [5,6], the equilibrium potentials of Ca–Pb alloys near operating temperature must be determined to effectively analyze the functionality of the Ca–Pb system for practical applications.

The cell potential of liquid Ca–Pb alloys was reported to be at 0.50–0.69 V by Delcet et al. who employed a thin single-crystal CaF_2 electrolyte for coulometric titration of Ca into liquid Pb at 1073 K [4]; however, was found to be significantly higher at 0.69–0.96 V by Kumar and Fray who employed a binary $\text{CaO–Al}_2\text{O}_3$ electrolyte at 1173 K [7]. This discrepancy translates to about a 2–3 orders of magnitude difference in the thermodynamic activity of Ca in Pb, and must be resolved as both data were considered in the assessment of the Ca–Pb phase diagram by Idbenali et al. [8] with preference given to the results by Delcet et al.

^{*} Corresponding author.

E-mail addresses: nds174@psu.edu (N.D. Smith), nicoleorabona@gmail.com (N.E. Orabona), jfp21@psu.edu (J.P. Soldan Palma), yxk42@psu.edu (Y. Kong), cfb5266@psu.edu (C. Blanchard), huk29@psu.edu (H. Kim).

¹ Indicates shared first-authorship.

<https://doi.org/10.1016/j.jpowsour.2020.227745>

Received 24 September 2019; Received in revised form 7 January 2020; Accepted 11 January 2020

Available online 3 February 2020

0378-7753/© 2020 Elsevier B.V. All rights reserved.

[4] without scientific justification.

This study investigated the equilibrium cell potentials of Ca–Pb alloys for use as a positive electrode in a Ca-based liquid metal battery by measuring their electromotive force (emf) versus pure Ca at 700–1060 K to provide data closer to the operating temperature of liquid metal batteries, as well as to resolve the discrepancy in the previously determined thermodynamic properties of Ca–Pb electrodes. In this work, we employed a sintered CaF_2 electrolyte which has been widely applied for reliable emf measurements of Ca alloys [9] due to its high ionic conductivity ($1.5 \times 10^{-3} \text{ S cm}^{-1}$ at 1073 K) and minimal electronic conduction [10]. In contrast to the previous works, this work utilized Ca–Pb alloy electrodes at fixed mole fractions (x_{Ca}) to allow for emf measurements over a wide range of temperatures as opposed to a singular temperature by eliminating the need for coulometric titration, in complement with their thermal and structural characterization. The emf values of six alloy compositions were measured simultaneously in the CaF_2 electrolyte to accelerate the experimental process.

The temperature-dependent thermodynamic properties of Ca–Pb alloys ($x_{\text{Ca}} = 0.06\text{--}0.80$) between 700 K and 1060 K were investigated by measuring open-circuit potential using the two-electrode electrochemical cell:



where pure Ca(s) served as a reference electrode (RE), solid CaF_2 as an electrolyte, and various compositions of Ca–Pb alloys as the working electrode (WE). The half-cell reactions for this cell are given by:



and the overall cell reaction is:



For this reaction, the change in partial molar Gibbs energy of Ca is:

$$\Delta \bar{G}_{\text{Ca}} = \bar{G}_{\text{Ca(in Pb)}} - G_{\text{Ca(s)}}^0 = RT \ln a_{\text{Ca}} \quad (5)$$

where $\bar{G}_{\text{Ca(in Pb)}}$ is the chemical potential of Ca in Pb, $G_{\text{Ca(s)}}^0$ is the standard chemical potential of pure Ca, a_{Ca} is the activity of Ca in Pb, R is the gas constant, and T is the temperature. The emf of this cell (E_{cell}) is directly related to $\Delta \bar{G}_{\text{Ca}}$ by the Nernst equation:

$$E_{\text{cell}} = \frac{-\Delta \bar{G}_{\text{Ca}}}{2F} = - \left(\frac{RT}{2F} \right) \ln a_{\text{Ca}}, \quad (6)$$

where F is the Faraday constant.

2. Experimental

2.1. Fabrication of electrochemical cell components

Electrolyte: The solid CaF_2 electrolyte for emf measurements was prepared from CaF_2 powder (99.5%, Alfa Aesar-11055) by ball milling 350 g powder mixed with 25 g polyvinyl alcohol binder (Sigma Aldrich-450030) and 1 L of isopropyl alcohol for 24 h. The mixture was dried in air for 24 h, then 130 g of the mixture was uniaxially pressed under approximately 30 MPa for 5 min into a green pellet (75 mm diameter, 17 mm thickness). Seven wells (11.2 mm diameter, 12 mm depth) were drilled into the pellet with one well in the center and six wells evenly spaced 25.4 mm away from the center (Fig. 1). Electrolyte caps (19 mm diameter, 10 mm height) were also pressed from 4 g of the mixture each with a 1.1 mm hole drilled through the center for the insertion of a W electrical lead. The fabricated pellets and caps were heated in a furnace at 373 K for 12 h to remove moisture, at 543 K for 12 h to burn off the polyvinyl alcohol binder, and at 1273 K for 3 h to sinter.

Electrodes: Pure Ca and Ca–Pb alloy electrodes were fabricated using

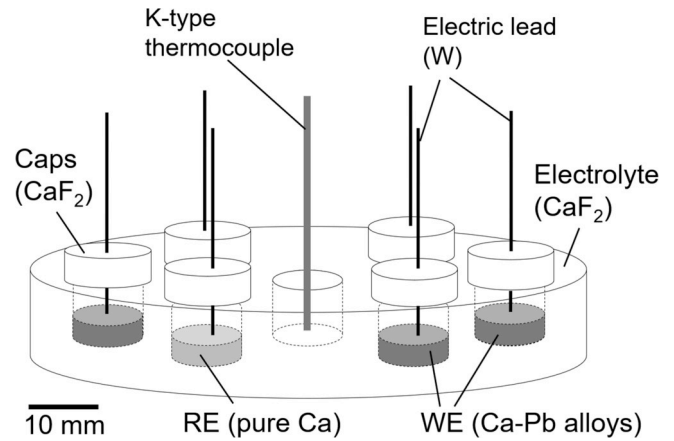


Fig. 1. Schematic of electrochemical cell for emf measurements of Ca–Pb alloys: $\text{Ca(s)} \mid \text{CaF}_2(\text{s}) \mid \text{Ca(in Pb)}$, where pure Ca is the reference electrode (RE) and each Ca–Pb alloy is the working electrode (WE). A typical emf cell included two pure Ca REs and four Ca–Pb WEs.

an arc-melter (MAM-1, Edmund Bühler GmbH) from Ca (99.5%, Alfa Aesar-10127) and Pb (99.9%, Sigma Aldrich-396117) pieces under an inert Ar atmosphere at given compositions. The electrodes were machined into a cylindrical shape (10 mm diameter, 7 mm height) with a 1.1 mm center hole for insertion of the electrical lead. Brittle Ca–Pb alloys at $x_{\text{Ca}} = 0.45\text{--}0.66$ were not machinable, instead, these alloys were re-melted using an induction heater (IH15A-2T, Across International) and electrical contact was established by immersing a W wire into the liquid Ca–Pb alloys. The compositions of the Ca–Pb alloys were analyzed using inductively coupled plasma atomic emission spectroscopy (ICP-AES, Perkin-Elmer Optima 5300DV) with a precision of 4% of the measured value.

2.2. Electrochemical cell assembly and emf measurements

The electrochemical cell was assembled in an Ar-filled glovebox ($\text{O}_2 < 0.5 \text{ ppm}$) to prevent the oxidation of the Ca metals and alloys. Two pure Ca metals (RE) and four Ca–Pb alloys (WE) at given compositions were placed in electrolyte wells and a K-type thermocouple was placed at the center well (Fig. 1). The solid CaF_2 electrolyte was placed in an alumina crucible (8.2 cm diameter, 3.0 cm height) inside a stainless-steel test chamber. Tungsten wires (46 cm length, 1 mm diameter) were polished with sandpaper, cleaned with acetone, and inserted into insulating alumina tubes (6.4 mm diameter) which were sealed at the top with epoxy. The W electrical leads were inserted into electrodes through a stainless-steel top flange and through the electrolyte caps. The electrolyte caps cover the electrodes to suppress cross-contamination through vapor-phase transport during the measurements. The test chamber was sealed inside the glovebox and loaded into a crucible furnace.

The sealed test chamber was evacuated ($< 1.0 \text{ Pa}$), heated under vacuum at 373 K for 10 h and at 543 K for 10 h to remove residual moisture and oxygen, and purged three times with high purity Ar. The chamber was heated to 1133 K for 0.3 h under flowing Ar (10 mL min^{-1}) to melt the electrodes and to establish electrical contact between the electrodes and electrolyte, then cooled to 1073 K for emf measurements. Measurements were taken in 25 K increments between 1073 K and 723 K; each temperature increment was held for 1.5 h and the cooling rate between steps was 5 K min^{-1} . The temperature of the cell was measured using a thermocouple (ASTM type-K) and thermocouple data acquisition system (NI 9211, National Instruments). Emf data were collected during each thermal cycle by measuring the potential difference between the RE and each Ca–Pb WE sequentially in 180 s intervals using a potentiostat-galvanostat (Autolab PGSTAT302 N, Metrohm AG) with a

multiplexer switching unit (MUX.SCN16). The potential difference between the two pure Ca electrodes was less than 5 mV throughout the measurement.

2.3. Thermal and structural characterization of Ca–Pb alloys

Phase transition temperatures were determined by differential scanning calorimetry (DSC) using a thermal analyzer (Netzsch, STA 449 F3 Jupiter). Approximately 20–50 mg of Ca–Pb alloy ($x_{\text{Ca}} = 0.06\text{--}0.80$) was placed in an alumina sample crucible with tungsten foil interlayer to prevent direct reaction between the Ca–Pb alloy and the alumina. Thermograms were gathered from both heating and cooling cycles with scan rates of 5–20 K min^{−1} under high purity Ar flow. The phase transition temperatures were determined from the onset temperatures for solidus transitions and from end-point temperatures for liquidus transitions during the heating cycle by extrapolating to a 0 K min^{−1} scan rate [11].

The phase constituents of the Ca–Pb alloys were analyzed utilizing powder X-ray diffraction (XRD, PANalytical Empyrean) over 2θ angles 20–75° at room temperature. The arc-melted alloys were heat treated for 24 h at 15 K below solidus temperature under inert Ar atmosphere to equilibrate phase constituents. The annealed alloys were cut into small pieces and coated in mineral oil inside a glove box to minimize oxidation for the XRD measurements. The mineral oil coating resulted in a broad background spectrum at low angles ($2\theta < 20^\circ$) that was subtracted for phase analysis.

3. Results and discussion

3.1. Emf measurements of Ca–Pb alloys

The emf values of Ca–Pb alloys vs. Ca(s) were measured between 700 and 1060 K in 25 K increments over a wide composition range of $x_{\text{Ca}} = 0.06\text{--}0.80$ (Fig. 2a). The measured emf values at a given temperature decreased as x_{Ca} increased (Nernst equation), approaching zero for $x_{\text{Ca}} = 0.80$ where pure Ca solid or Ca-rich liquid phases are present. Fig. 2b provides a zoomed-in version of the emf measurements for liquid Ca–Pb alloys at low x_{Ca} , which are most relevant for liquid metal batteries. At 873 K, theoretical cell voltages of liquid Ca–Pb alloys (vs. pure Ca) range from 0.57 to 0.62 V with liquidus composition at $x_{\text{Ca}} = \sim 0.16$. For $x_{\text{Ca}} = 0.06\text{--}0.26$, the emf values changed linearly in the liquid state and merged onto a curve in the [L + CaPb₃] two-phase region where the activity (a_{Ca}) is invariant respective to x_{Ca} (Gibbs phase rule), suggesting their equilibrium phase behavior. Similar two-phase behavior was

observed for $x_{\text{Ca}} = 0.33\text{--}0.45$ in the [CaPb₃ + CaPb] region below 900 K and the [L + CaPb] region. The discontinuities in the slope (dE_{cell}/dT) are due to the first-order transition reactions of these alloys.

Mole fraction $x_{\text{Ca}} = 0.26$ would exhibit a two-phase equilibrium of [CaPb₃ + CaPb] below the solidus (900 K) and result in a similar emf trajectory to that of $x_{\text{Ca}} = 0.33\text{--}0.45$; however, the emf trajectory of $x_{\text{Ca}} = 0.26$ was located between those of [L + CaPb₃] and [CaPb₃ + CaPb] implying non-equilibrium phase transitions during the cooling cycle (Fig. 2b). Mole fractions of $x_{\text{Ca}} = 0.55$ and 0.59 would possess two equilibrium phases (CaPb + Ca₅Pb₃) below solidus and thus a similar emf trajectory; however, the emf trajectories deviated from each other due to a non-equilibrium phase transition. A similar non-equilibrium emf trajectory was also found for $x_{\text{Ca}} = 0.76$ and 0.80 below solidus.

Overall, the emf measurements were most reliable for $x_{\text{Ca}} = 0.06\text{--}0.45$, especially in the presence of a liquid phase. Emf measurements of high Ca mole fractions ($x_{\text{Ca}} > 0.45$) exhibited limited stability possibly due to the formation of non-equilibrium phases during the thermal cycle and/or the high melting temperatures (>1247 K for $x_{\text{Ca}} = 0.55\text{--}0.66$ [8]) which compromise electrical contact with the electrolyte. The phase constituents and transition temperatures of Ca–Pb alloys were further investigated to complement emf measurements by thermal and structural analyses using DSC and XRD for selected mole fractions.

3.2. Thermal and structural characterization of Ca–Pb alloys

Phase transition temperatures of Ca–Pb alloys ($x_{\text{Sr}} = 0.06\text{--}0.80$) were determined from DSC measurements at heating rates of 5–20 K min^{−1}. Representative thermograms are presented in Fig. 3 at a heating rate of 20 K min^{−1}, where four characteristic transitions (I–IV) and liquidus transitions (*) are indicated. The analyzed transition temperatures at each mole fraction are summarized in Table 1 and overlaid on the most recently assessed Ca–Pb phase diagram (Fig. 4) by Idbenali et al. [8]. In addition, transition temperatures estimated from the discontinuity in emf slope for $x_{\text{Ca}} = 0.06\text{--}0.45$ (Fig. 2b) were included for comparison.

According to the phase diagram, the measured characteristic temperatures indicate four distinct eutectic transitions of [I: L = Pb + CaPb₃], [II: L = CaPb₃ + CaPb], [III: L = CaPb + Ca₅Pb₃], and [IV: L = Ca₂Pb + Ca]. The liquidus and eutectic (II) temperatures from DSC and emf measurements were in close agreement with each other as well as with the assessed phase diagram (Fig. 4), indicating reliable emf measurements. The liquidus temperature at $x_{\text{Ca}} = 0.45$ (1117 K) from DSC was substantially lower than the assessed phase diagram at ~ 1220 K, but agreed well with previous experimental works from Bruzzone et al. [13] and Baar et al. [12], suggesting a further refinement of

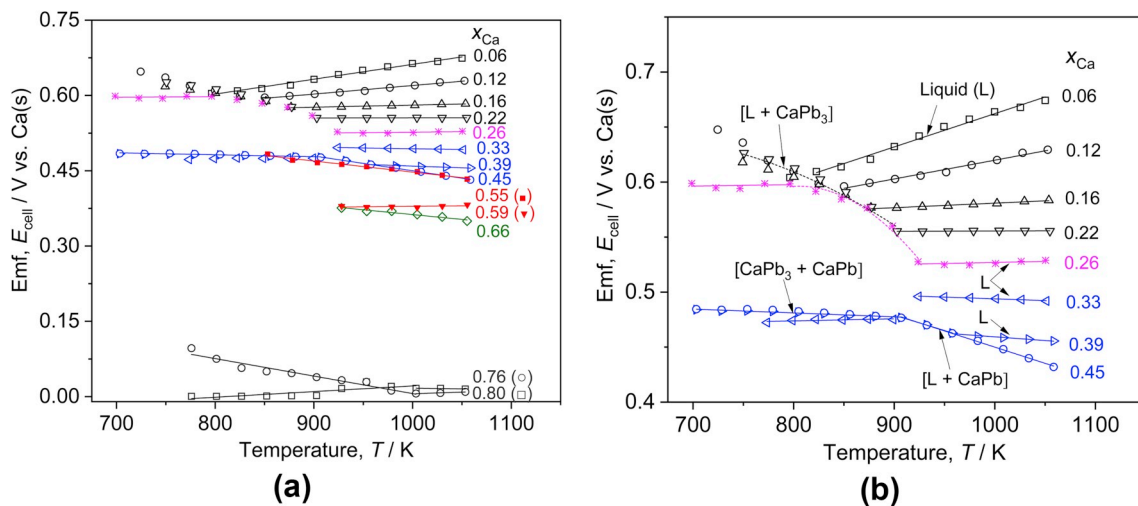


Fig. 2. Emf of Ca–Pb alloys versus pure Ca as a function of temperature for Ca–Pb alloys (a) $x_{\text{Ca}} = 0.06\text{--}0.80$ (b) $x_{\text{Ca}} = 0.06\text{--}0.45$, where solid lines represent linear fits and dashed lines are curved fits.

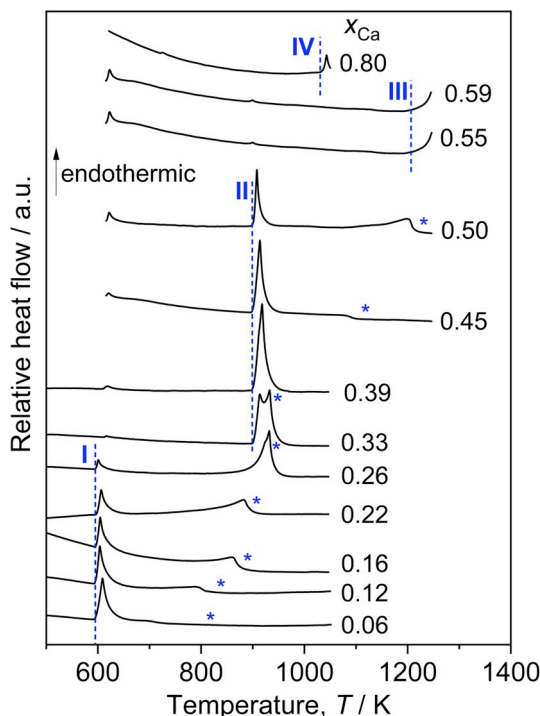


Fig. 3. DSC data collected upon heating Ca–Pb alloys $x_{\text{Ca}} = 0.06$ – 0.80 at 20 K min^{-1} , indicating phase transitions of liquidus temperatures (*) and eutectic temperatures (I–IV).

Table 1

Summary of the transition temperatures (T_{trs}) for each mole fraction from DSC measurements and the characteristic temperatures (I–IV) from the average of multiple compositions and by Idbenali et al. [8]. The standard errors in the parentheses represent the 95% confidence interval of the fit.

x_{Ca}	T_{trs} (K)				liquidus
	I	II	III	IV	
0.06	594 (± 3)	–	–	–	815 (± 13)
0.12	592 (± 4)	–	–	–	838 (± 5)
0.16	593 (± 1)	–	–	–	888 (± 2)
0.22	596 (± 2)	–	–	–	904 (± 3)
0.26	596 (± 3)	904 (± 14)	–	–	939 (± 1)
0.33	609 (± 1) ^a	900 (± 2)	–	–	931 (± 3)
0.39	608 (± 2) ^a	899 (± 3)	–	–	–
0.45	609 (± 2) ^a	899 (± 3)	–	–	1117 (± 5)
0.50	608 (± 1) ^a	900 (± 3)	–	–	1229 (± 2)
0.55	609 (± 2) ^a	891 (± 1) ^a	1236 (± 5)	–	–
0.59	–	–	1240 (–)	–	–
0.80	–	–	–	1029 (± 2)	–
Average	594 (± 2)	900 (± 4)	1238 (± 2)	1029 (± 2)	–
Idbenali et al.	599	911	1241	1023	–

^a Indicates characteristic transition temperatures which were detected beyond equilibrium limit and were not included for calculating eutectic transition temperatures of I and II.

thermodynamic models for liquidus temperatures at $x_{\text{Ca}} = 0.33$ – 0.50 . During DSC measurements, eutectic (I) transition was observed for $x_{\text{Ca}} = 0.26$ – 0.55 well beyond equilibrium limit ($x_{\text{Ca}} = 0.25$); eutectic (II) transition for $x_{\text{Ca}} = 0.55$ – 0.59 beyond $x_{\text{Ca}} = 0.50$, indicating the formation of non-equilibrium phases during the thermal cycle.

The presence of non-equilibrium phases was also examined from XRD patterns of annealed Ca–Pb alloys by comparing to those of the reported crystal structures [14–16] (Fig. 5). It is noted that the XRD patterns of multi-phase alloys were too complex with overlapping peaks for detailed phase analysis and thus the analysis is limited to a qualitative description regarding the presence of non-equilibrium phases. For

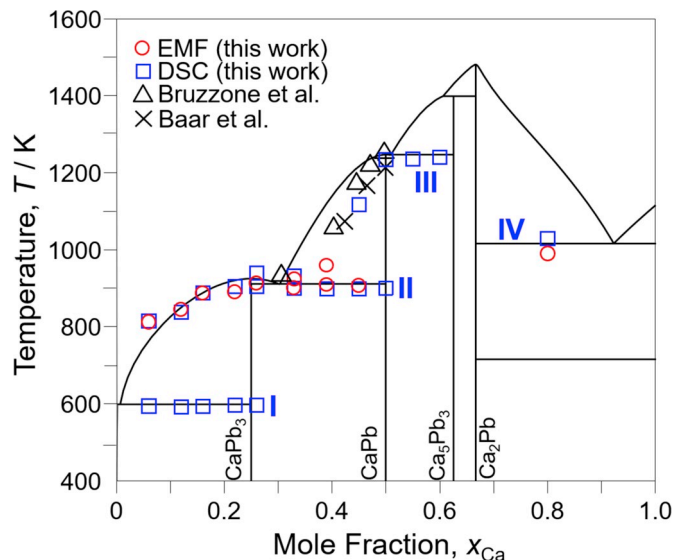


Fig. 4. Ca–Pb phase diagram reproduced using Thermo-Calc with the thermodynamic parameters specified in Idbenali et al. [8] with detected phase transitions from this work (emf and DSC) as well as selected transitions reported by Baar et al. and Bruzzone et al. [12,13].

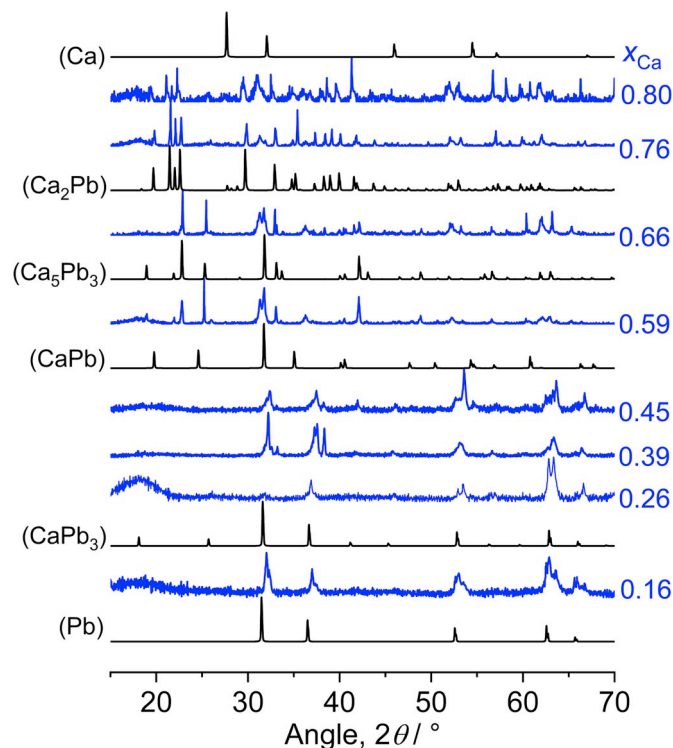


Fig. 5. Powder XRD patterns of Ca–Pb alloys compared to the reported diffraction patterns of Ca–Pb intermetallic compounds and pure metals [14–16].

example, the XRD pattern for $x_{\text{Ca}} = 0.76$ suggests the presence of non-equilibrium Ca_5Pb_3 phase. In addition, the XRD pattern of $x_{\text{Ca}} = 0.26$ was close to that of $x_{\text{Ca}} = 0.16$, suggesting its main phase constituents as $[\text{Pb} + \text{CaPb}_3]$ with little CaPb phase, qualitatively explaining the erratic emf trajectory of $x_{\text{Ca}} = 0.26$ which deviated from that of $x_{\text{Ca}} = 0.33$ – 0.45 (Fig. 2).

The complementary DSC and XRD measurements confirmed the phase transitions from the emf measurements as well as the formation of

non-equilibrium phases which resulted in erratic emf trajectory during the thermal cycle.

3.3. Thermochemical properties of Ca–Pb alloys

The temperature-dependent emf data were analyzed to calculate the change of the partial molar quantities of entropy ($\Delta\bar{S}_{Ca}$) and enthalpy ($\Delta\bar{H}_{Ca}$) using the Nernst and Gibbs-Helmholtz relations:

$$E_{cell} = -\frac{\Delta\bar{G}_{Ca}}{2F} = -\frac{\Delta\bar{H}_{Ca}}{2F} + T \frac{\Delta\bar{S}_{Ca}}{2F} \quad (7)$$

$$\Delta\bar{S}_{Ca} = -\left(\frac{\partial\Delta\bar{G}_{Ca}}{\partial T}\right)_p = 2F\left(\frac{\partial E_{cell}}{\partial T}\right)_p \quad (8)$$

$$\Delta\bar{H}_{Ca} = -T^2\left(\frac{\partial(\Delta\bar{G}_{Ca}/T)}{\partial T}\right)_p = -2F\left(\frac{\partial(E_{cell}/T)}{\partial(1/T)}\right)_p \quad (9)$$

For linear E_{cell} - T data (solid lines in Fig. 2), $\Delta\bar{S}_{Ca}$ and $\Delta\bar{H}_{Ca}$ were estimated from the slope (Eq. (8)) and the intercept at 0 K (Eq. (9)), respectively. The linear fits and related partial molar quantities are summarized in Table 2.

The estimated $\Delta\bar{H}_{Ca}$ values (~ -100 kJ mol⁻¹) at $x_{Ca} = 0.12$ –0.22 were in close agreement with the calorimetric measurements by Notin et al. [17]. The curved, non-linear data (dashed lines in Fig. 2) in the [L + CaPb₃] two-phase region were fit to the following general fitting equation:

$$E_{cell} = A + BT + CT \ln(T), \quad (10)$$

where A , B , and C are fitting parameters, summarized in Table 3.

The emf values of Ca–Pb alloys at 773–973 K were interpolated from the linear and curved fits of measured data, listed in Table 4, and were used to calculate the activity (a_{Ca}) and the excess partial molar Gibbs energy (\bar{G}_{Ca}^E),

$$\bar{G}_{Ca}^E = RT(\ln a_{Ca} - \ln x_{Ca}). \quad (11)$$

The activity of Ca in Pb is as low as 1.7×10^{-7} at $x_{Ca} = 0.06$ and 973 K, resulting in a large excess partial molar Gibbs energy ($\bar{G}_{Ca}^E = -103$ kJ mol⁻¹). These thermochemical properties as a function of x_{Ca} at 973 K are presented in Fig. 6, compared to the assessed properties by Idbenali et al. [8]. The emf value decreases as x_{Ca} increases in the liquid phase and remains constant in the [L + CaPb] region due to invariant activity in two-phase equilibrium. However, in the [CaPb + Ca₅Pb₃] region, the

Table 3

Non-linear fits of the temperature dependence of emf data in two-phase [L + CaPb₃] region. The data were fit to $E_{cell} = A + BT + CT \ln(T)$. The standard errors in the parentheses represent the 95% confidence interval of the fit.

x_{Ca}	T (K)	A	B	C	adj- R^2
0.06–0.22	751–902	−0.507 (±0.663)	0.013 (±0.006)	−1.77(±0.80) $\times 10^{-3}$	0.985
0.26	797–923	−5.739 (±1.712)	0.060 (±0.015)	−7.87(±1.99) $\times 10^{-3}$	0.969

emf values deviated from each other due to the formation of non-equilibrium phases during the measurements.

The measured emf values and solution properties at 973 K were in excellent agreement with the modeled results which incorporated the experimental results (emf values) of Ca–Pb alloys by Delcet et al. [4] at 1073 K. The emf values in this work were extrapolated to 1073 K and compared to the results by Delcet et al. (Fig. 7). The emf values from both works were in close agreement, in particular for the liquid phase region, demonstrating the reliability of a solid CaF₂ electrolyte for determining thermochemical properties of Ca–Pb alloys. In addition, both emf results indicate that the liquidus composition is likely to be higher than the assessed model at $x_{Ca} = 0.37$ based on continuously decreasing emf values up to $x_{Ca} = 0.40$, in agreement with the DSC results at $x_{Ca} = 0.33$ –0.50.

The measured emf values vs. pure Ca were extrapolated to 1173 K, above the melting temperature of pure Ca ($T_{m,Ca} = 1115$ K), and compared to the experimental results from the Kumar and Fray [7] (Fig. 8). For consistent comparison, the change in the reference state of pure Ca from solid to liquid was considered to a first approximation based on the Gibbs energy difference:

$$G_{Ca(l)}^0 - G_{Ca(s)}^0 = \Delta S_f(T_{m,Ca} - T) \quad (12)$$

where ΔS_f is the entropy of fusion of Ca ($= 7.65$ J mol⁻¹ K⁻¹) [18]. At $T = 1173$ K, the Gibbs energy difference was -443 J mol⁻¹, requiring a subtraction of the emf values by 2.3 mV from extrapolated values. As shown in Fig. 8, this work was in close agreement with the computationally assessed values within the same order of magnitude for activity values in liquid state (Fig. 8b); however, it diverged from the experimental results by Kumar and Fray where calcium magnetoplumbite (CaO–Al₂O₃, ht structure) was employed as the electrolyte for coulometric titration of Ca into liquid Pb: Ca(l) | Al₂O₃–CaO | Ca(in Pb) [7]. In principle, the emf measurements of Ca–Pb alloys vs. pure Ca should be

Table 2

Changes in partial molar entropy ($\Delta\bar{S}_{Ca}$) and partial molar enthalpy ($\Delta\bar{H}_{Ca}$) of Ca, calculated from linear fits of E_{cell} versus T , where $\partial E_{cell}/\partial T$ and $\partial(E_{cell}/T)/\partial(1/T)$ are the slope and intercept, respectively. The standard errors in the parentheses represent the 95% confidence interval of the fit.

x_{Ca}	T (K)	$\partial E_{cell}/\partial T$ (μV K ⁻¹)	$\partial(E_{cell}/T)/\partial(1/T)$ (mV)	$\Delta\bar{S}_{Ca}$ (J mol ⁻¹ K ⁻¹)	$\Delta\bar{H}_{Ca}$ (kJ mol ⁻¹)	adj- R^2
0.06	796–1050	303 (±12)	360 (±10)	58.4	−69	0.985
0.12	850–1053	171 (±8)	449 (±8)	32.9	−87	0.983
0.16	877–1054	42 (±4)	539 (±3)	8.0	−104	0.951
0.22	903–1055	3 (±2)	552 (±2)	0.6	−107	0.327
0.26	924–1050	19 (±16)	508 (±15)	3.7	−98	0.091
0.33	774–899	19 (±8)	458 (±6)	3.7	−88	0.510
	924–1051	−32 (±2)	526 (±2)	−6.1	−101	0.972
0.39	703–907	−35 (±3)	509 (±2)	−6.8	−98	0.945
	907–983	−279 (±12)	731 (±11)	−53.9	−141	0.996
	983–1058	−68 (±6)	527 (±6)	−13.1	−102	0.972
0.45	703–907	−39 (±5)	513 (±4)	−7.6	−99	0.896
	907–1058	−295 (±5)	745 (±5)	−56.8	−144	0.998
0.55	853–1055	−221 (±12)	668 (±11)	−42.6	−129	0.977
0.59	928–1055	20 (±17)	359 (±17)	4.0	−69	0.069
0.66	928–1055	192 (±21)	555 (±21)	−37.1	−107	0.943
0.76	776–1003	−349 (±29)	355 (±26)	−67.3	−68	0.940
	1003–1053	66 (±15)	−60 (±15)	12.8	12	0.906
0.80	776–1003	113 (±29)	−92 (±26)	21.8	18	0.617
	1003–1053	−31 (±17)	48 (±17)	−6.0	−9	0.544

Table 4

Measured emf (E_{cell}), natural log activity of calcium ($\ln a_{\text{Ca}}$), and excess partial molar Gibbs energy ($\bar{G}_{\text{Ca}}^{\text{E}}$) of Ca–Pb alloys ($x_{\text{Ca}} = 0.06\text{--}0.80$) at 773, 873, and 973 K.

x_{Ca}	E_{cell} (V)			$\ln a_{\text{Ca}}$			$\bar{G}_{\text{Ca}}^{\text{E}}$ (kJ mol ^{−1})		
	773 K	873 K	973 K	773 K	873 K	973 K	773 K	873 K	973 K
0.06	0.614	0.624	0.654	−18.4	−16.6	−15.6	−100	−100	−103
0.12	0.614	0.598	0.615	−18.4	−15.9	−14.7	−105	−100	−102
0.16	0.614	0.576	0.580	−18.4	−15.3	−13.8	−107	−98	−97
0.22	0.614	0.567	0.556	−18.4	−15.1	−13.3	−109	−98	−95
0.26	0.597	0.560	0.526	−17.9	−14.9	−12.5	−107	−98	−91
0.33	0.473	0.475	0.495	−14.2	−12.6	−11.8	−84	−84	−87
0.39	0.482	0.478	0.476	−14.5	−12.7	−11.4	−87	−85	−84
0.45	0.483	0.479	0.487	−14.5	−12.7	−11.6	−88	−87	−88
0.55	0.497	0.475	0.453	−14.9	−12.6	−10.8	−92	−87	−83
0.59	0.374	0.377	0.379	−11.2	−10.0	−9.0	−69	−69	−69
0.66	0.406	0.384	0.365	−12.2	−10.2	−8.7	−76	−71	−67
0.76	0.085	0.002	0.020	−2.6	−0.1	−0.5	−15	1	−2
0.80	−0.004	0.047	0.012	0.1	−1.2	−0.3	3	−7	0

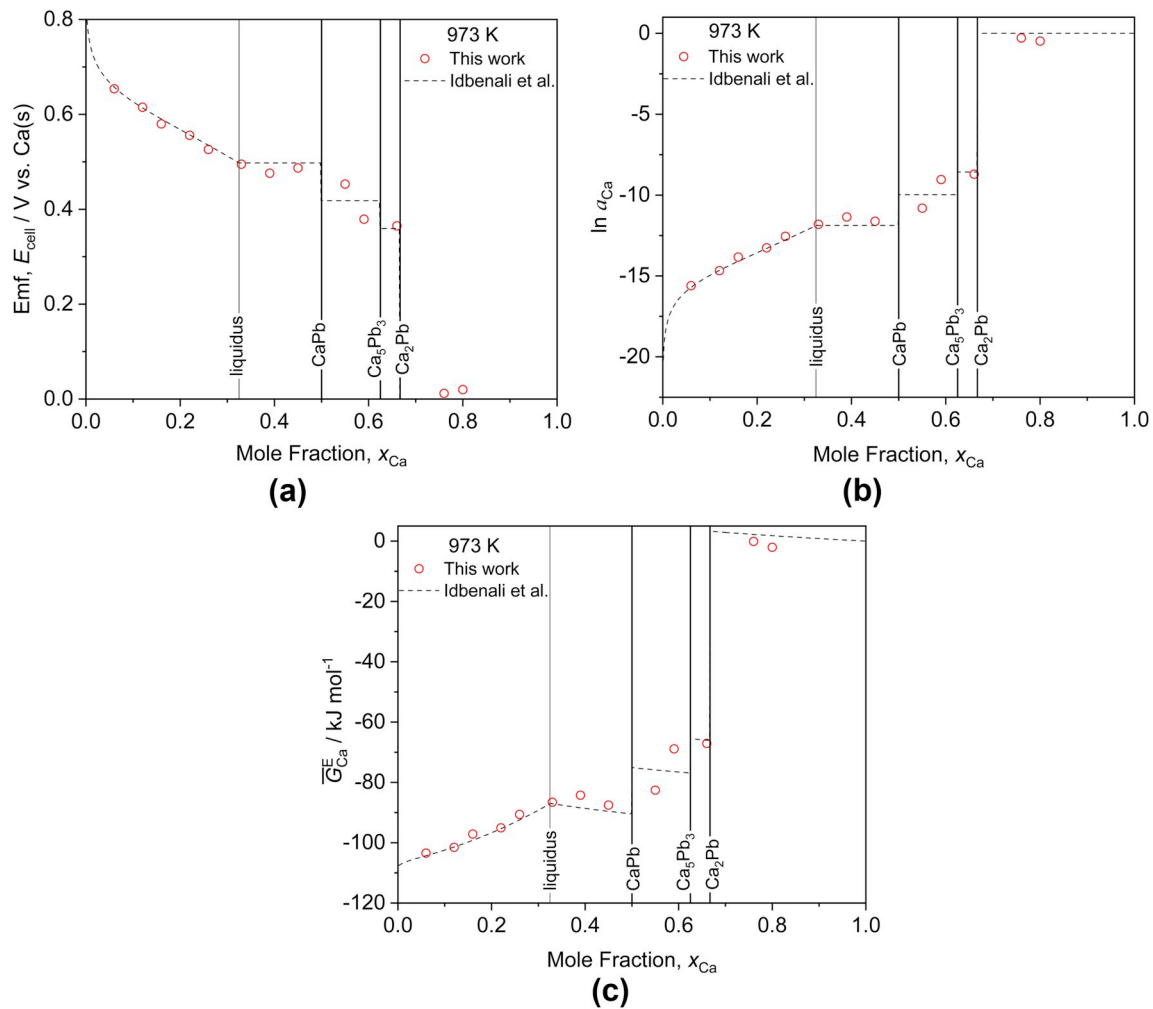
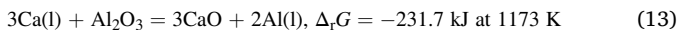


Fig. 6. (a) Measured emf values (E_{cell}), (b) natural log of activity of calcium ($\ln a_{\text{Ca}}$), and (c) excess partial molar Gibbs energy as a function of x_{Ca} at 973 K alongside assessed values from Idbenali et al. [8]. The liquidus composition was obtained from the assessed phase diagram.

independent of electrolyte choice (Eq. (6)) assuming half-cell reactions are in electrochemical equilibrium under open-circuit condition. From this perspective, the use of liquid Ca(l) might result in reaction with the oxide electrolyte spontaneously [19] according to:



, which would compromise the emf measurements with this side

reaction.

4. Conclusions

This study determined the thermodynamic properties of the binary Ca–Pb system via emf measurements, including activity and partial molar quantities (entropy and enthalpy) at temperatures more suitable

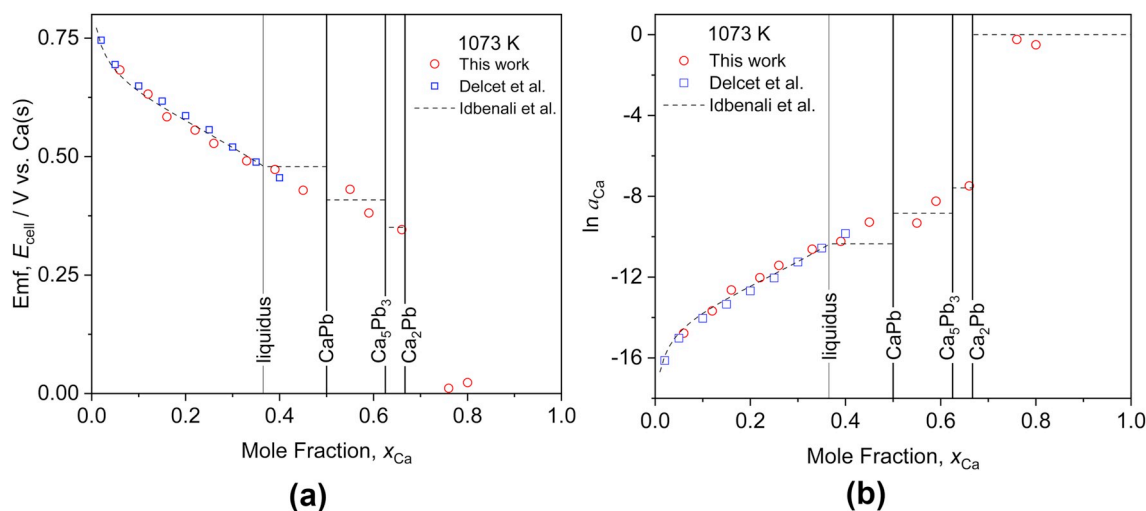


Fig. 7. (a) Measured emf values (E_{cell}) and (b) natural log of activity of calcium ($\ln a_{\text{Ca}}$) as a function of x_{Ca} at 1073 K alongside assessed values from Idbenali et al. and the experimental results by Delcet et al. [4,8]. The liquidus composition was obtained from the assessed phase diagram.

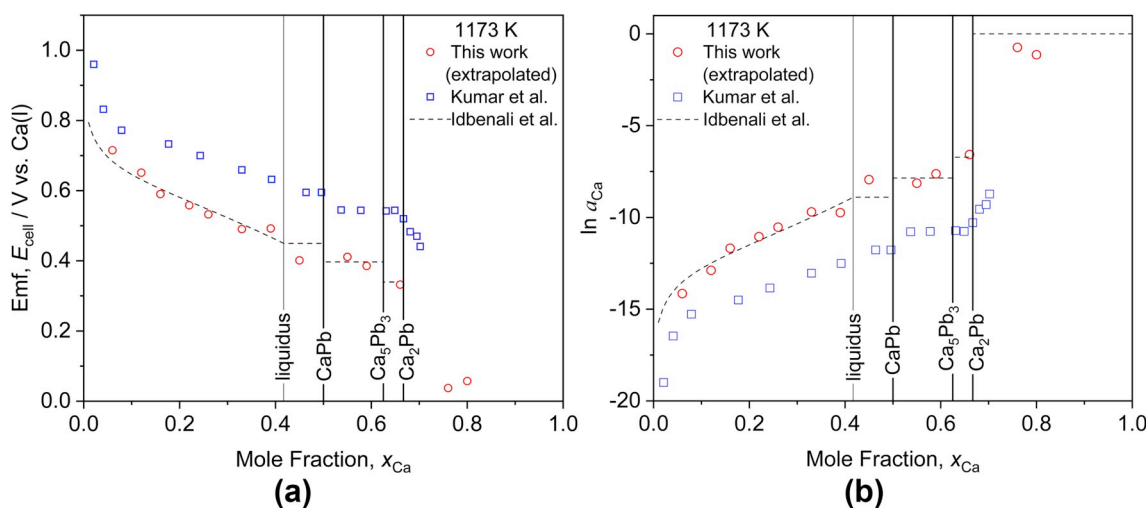


Fig. 8. (a) Measured emf values (E_{cell}) and (b) natural log of activity of calcium ($\ln a_{\text{Ca}}$) as a function of x_{Ca} at 1173 K alongside assessed values from Idbenali et al. and the experimental results by Kumar and Fray [7,8]. The liquidus composition was obtained from the assessed phase diagram.

for liquid metal battery operation ($T < 873$ K) in complement with DSC and XRD measurements for thermal and phase characterization. The emf results were in excellent agreement with the results from Delcet et al. [4] at 1073 K whose results were incorporated into the thermodynamic description of the Ca–Pb system by Idbenali et al. [8]. The discrepancy between Delcet et al. at 1073 K [4] and Kumar and Fray at 1173 K [7] is believed to be due to their selection of electrolyte system, as the use of an oxide-based electrolyte is thought to result in a side reaction with pure Ca(l) and compromise the emf measurements of Ca–Pb alloys.

At 873 K, the liquid Ca–Pb alloys resulted in an open-circuit cell voltage of 0.57–0.62 V vs. Ca(s) with a liquid-state solubility at $x_{\text{Ca}} = 0.16$. The relatively low cell voltage of the Ca–Pb alloys coupled with a low materials cost may suggest the utility of Pb as an alloying element with high-voltage electrode materials such as Sb ($E_{\text{cell}} = 0.98$ –1.15 V vs. Ca [20]) to develop low-melting, low-cost electrodes for Ca-based liquid metal batteries.

Author contributions

The manuscript was written through contributions of all authors. All authors have given approval to the final version of the manuscript.

Funding sources

US Department of Energy, Office of Nuclear Energy.
US National Science Foundation.

Declaration of competing interest

The authors declare that they have no known competing financial interests or personal relationships that could have appeared to influence the work reported in this paper.

Acknowledgements

This work was supported by the US National Science Foundation (grant number: CMMI-1662817) and the US Department of Energy, Office of Nuclear Energy's Nuclear Energy University Programs (Award No. DE-NE0008757).

Appendix A. Supplementary data

Supplementary data to this article can be found online at <https://doi.org/10.1016/j.jpowsour.2020.227745>.

org/10.1016/j.jpowsour.2020.227745.

References

- [1] K. Wang, K. Jiang, B. Chung, T. Ouchi, P.J. Burke, D.A. Boysen, D.J. Bradwell, H. Kim, U. Muecke, D.R. Sadoway, Lithium-antimony-lead liquid metal battery for grid-level energy storage, *Nature* 514 (2014) 348–350, <https://doi.org/10.1038/nature13700>.
- [2] L.S. Kanevskii, V.S. Dubasova, Degradation of lithium-ion batteries and how to fight it: a review, *Russ. J. Electrochem.* 41 (2005) 1–16, <https://doi.org/10.1007/s11175-005-0001-7>.
- [3] H. Kim, D.A. Boysen, J.M. Newhouse, B.L. Spatocco, B. Chung, P.J. Burke, D. J. Bradwell, K. Jiang, A.A. Tomaszowska, K. Wang, W. Wei, L.A. Ortiz, S.A. Barriga, S.M. Poizeau, D.R. Sadoway, Liquid metal Batteries : past, present, and future, *Chem. Rev.* 113 (2013) 2075–2099, <https://doi.org/10.1021/cr300205k>.
- [4] J. Delcet, A. Delgado-Brune, J.J. Egan, Coulometric titrations using CaF_2 and BaF_2 solid electrolytes to study alloy phases, in: Y.A. Chang, J.F. Smith (Eds.), *Symp. Calc. Phase Diagrams Thermochemistry Alloy Phases*, Metallurgical Society of AIME, Milwaukee, 1979, pp. 275–287.
- [5] T. Ouchi, H. Kim, B.L. Spatocco, D.R. Sadoway, Calcium-based multi-element chemistry for grid-scale electrochemical energy storage, *Nat. Commun.* 7 (2016) 1–5, <https://doi.org/10.1038/ncomms10999>.
- [6] T. Ouchi, H. Kim, X. Ning, D.R. Sadoway, Calcium-Antimony alloys as electrodes for liquid metal batteries, *J. Electrochem. Soc.* 161 (2014) 1898–1904, <https://doi.org/10.1149/2.0801412jes>.
- [7] R.V. Kumar, D.J. Fray, Electrochemical determination of the thermodynamics of the Ca-Pb system at 1173 K using calcium magnetoplumbite as the electrolyte, *Scand. J. Metall.* 22 (1993) 266–270.
- [8] M. Idbenali, C. Servant, N. Selhaoui, L. Bouriden, A thermodynamic reassessment of the Ca-Pb system, *J. Phase Equilibria* 32 (2008) 64–73, <https://doi.org/10.1361/105497101770339265>.
- [9] H. Ipser, A. Mikula, I. Katayama, Overview: the emf method as a source of experimental thermodynamic data, *Calphad Comput. Coupling Phase Diagrams Thermochem* (2010), <https://doi.org/10.1016/j.calphad.2010.05.001>.
- [10] J. Delcet, R.J. Heus, J.J. Egan, Electronic conductivity in solid CaF_2 at high temperature, *J. Electrochem. Soc. Solid State Sci. Technol.* 125 (1976), 369–217.
- [11] W.J. Boettinger, U.R. Kattner, K.W. Moon, J.H. Perepezko, DTA and heat-flux DSC measurements of alloy melting and freezing, *Methods Phase Diagr. Determin.* (2007) 151–221, <https://doi.org/10.1016/B978-008044629-5/50005-7>.
- [12] N. Baar, Alloys of Mo with Ni, Mn with Th, and Ca with Mg, Ti, Pb, Cu, and Ag, *Z. Anorg. Chem.* 70 (1911) 372–377.
- [13] G. Bruzzone, F. Merlo, The equilibrium phase diagram of the calcium-lead system and crystal structures of the compounds CaPb , EuPb and YbPb , *J. Less Common. Met.* 48 (1976) 103–109, [https://doi.org/10.1016/0022-5088\(76\)90236-8](https://doi.org/10.1016/0022-5088(76)90236-8).
- [14] G. Bergerhoff, I.D. Brown, *Inorganic Crystal Structure Database* (FIZ Karlsruhe), 1978.
- [15] L.D. Calvert, P. Villars, *Pearson's Handbook of Crystallographic Data for Intermetallic Phases*, ASM, Mater. Park. OH, 1991.
- [16] R.T. Downs, M. Hall-Wallace, *The American mineralogist crystal structure database*, *Am. Mineral.* 88 (2003) 247–250.
- [17] M. Notin, L. Bouriden, E. Belbacha, J. Hertz, Enthalpies et Diagramme de Phases du Systeme Ca-Pb, *J. Less Common. Met.* 154 (1989) 121–135.
- [18] W.M. Haynes, *CRC Handbook of Chemistry and Physics*, 97th Edition, 2017. <http://hbcponline.com/faces/contents/InteractiveTable.xhtml>.
- [19] A. Roine, Outokumpu HSC Chemistry for Windows. Chemical Reaction and Equilibrium Software with Extensive Thermochemical Database, Outokumpu Research OY, Pori, 2002.
- [20] S. Poizeau, H. Kim, J.M. Newhouse, B.L. Spatocco, D.R. Sadoway, Determination and modeling of the thermodynamic properties of liquid calcium-antimony alloys, *Electrochim. Acta* (2012), <https://doi.org/10.1016/j.electacta.2012.04.139>.